A&A 574, A64 (2015)
DOI: 10.1051/0004-6361/201424883

Astronomy & Astrophysics

Properties of the solar neighbor WISE J072003.20−084651.2⋆

V. D. Ivanov[1], P. Vaisanen[2,3], A. Y. Kniazev[2,3,4], Y. Beletsky[5], E. E. Mamajek[6], K. Mužić[1], J. C. Beamín[1,7], H. M. J. Boffin[1], D. Pourbaix[8,⋆⋆], P. Gandhi[9,10], A. Gulbis[2,3], L. Monaco[1], I. Saviane[1], R. Kurtev[11,12], D. Mawet[1], J. Borissova[11,12], and D. Minniti[12,13]

[1] European Southern Observatory, Ave. Alonso de Cordova 3107, Casilla 19001 Santiago 19, Chile
e-mail: vivanov@eso.org
[2] South African Astronomical Observatory, PO Box 9, 7935 Observatory, Cape Town, South Africa
[3] Southern African Large Telescope Foundation, PO Box 9, 7935 Observatory, Cape Town, South Africa
[4] Sternberg Astronomical Institute, Lomonosov Moscow State University, 119992 Moscow, Russia
[5] Las Campanas Observatory, Carnegie Institution of Washington, Colina el Pino, Casilla 601 La Serena, Chile
[6] Department of Physics and Astronomy, University of Rochester, Rochester, NY 14627, USA
[7] Instituto de Astrofísica, Facultad de Física, Pontificia Universidad Católica de Chile, Casilla 306 Santiago 22, Chile
[8] Institut d'Astronomie et d'Astrophysique, Université Libre de Bruxelles (ULB), 1050 Bruxelles, Belgium
[9] Department of Physics, Durham University, South Road, Durham DH1 3LE, UK
[10] School of Physics & Astronomy, University of Southampton, Highfield, Southampton SO17 1BJ, UK
[11] Instituto de Física y Astronomía, Universidad de Valparaiso, Av. Gran Bretaña 1111, Casilla 5030 Playa Ancha, Chile
[12] Millennium Institute of Astrophysics (MAS), 36-D Casilla Santiago, Chile
[13] Departamento de Ciencias Físicas, Universidad Andres Bello, Av. Republica 252, 8370251 Santiago, Chile

Received 30 August 2014 / Accepted 24 October 2014

ABSTRACT

Context. The severe crowding towards the Galactic plane suggests that the census of nearby stars in that direction may be incomplete. Recently, Scholz reported a new M9 object at an estimated distance $d \simeq 7$ pc (WISE J072003.20−084651.2; hereafter WISE J0720) at Galactic latitude $b = 2.3°$.

Aims. Our goals are to determine the physical characteristics of WISE J0720, its kinematic properties, and to address the question of whether it is a binary object, as was suggested in the discovery paper.

Methods. Optical and infrared spectroscopy from the Southern African Large Telescope and *Magellan*, respectively, and spectral energy distribution fitting were used to determine the spectral type of WISE J0720. The measured radial velocity, proper motion, and parallax yielded its Galactic velocities. We also investigated if WISE J0720 may show X-ray activity based on archival data.

Results. Our spectra are consistent with spectral type L0 ± 1. We find no evidence for binarity, apart from a minor 2σ level difference in the radial velocities taken at two different epochs. The spatial velocity of WISE J0720 does not connect it to any known moving group; instead, it places the object with high probability in the old thin disk or in the thick disk. The spectral energy distribution fit hints at excess in the 12 μm and 22 μm WISE bands which may be due to a redder companion, but the same excess is visible in other late-type objects, and it more likely implies a shortcoming of the models (e.g., problems with the effective wavelengths of the filters for these extremely cool objects, etc.) rather than a disk or redder companion. The optical spectrum shows some Hα emission, indicative of stellar activity. Archival X-ray observations yield no detection.

Conclusions. WISE J0720 is a new member of the solar neighborhood, the third nearest L dwarf. Our data do not support the hypothesis of its binary nature.

Key words. stars: distances – solar neighborhood – stars: low-mass – stars: individual: WISE J072003.20–84651.2 – proper motions – stars: individual: 2MASS J07200708–0845589

1. Introduction

Recently, Scholz (2014) reported the discovery of a new nearby M-type star, WISE J072003.20−084651.2 (hereafter, WISE J0720), demonstrating yet again that our knowledge of the late-type stellar content of the solar neighborhood is incomplete. Other new nearby ($D \leq 10$ pc), low-mass mass objects discovered in the solar neighborhood include those reported by Artigau et al. (2010); Lucas et al. (2010); Scholz et al. (2011, 2014); Luhman (2013, 2014), among others. Nearby examples of low-mass stellar and substellar objects are important targets for understanding stellar interiors near the hydrogen-burning limit (Dieterich et al. 2014), the diversity of stellar and substellar atmospheres and testing atmospheric models (e.g., Leggett et al. 2010), initial mass function (e.g., Kirkpatrick et al. 2011), activity trends (e.g., Berger et al. 2010), the multiplicity and formation of low-mass objects (e.g., Faherty et al. 2010; Dieterich et al. 2012), and providing bright low-mass targets for planet surveys (e.g., Blake et al. 2010).

Typically, the missed objects are cool, making the Wide-field Infrared Survey Explorer (WISE; Wright et al. 2010) satellite an excellent tool for discovering them. Indeed, Scholz (2014) used color and proper motion criteria based on WISE and 2MASS (Two Micron All Sky Survey; Skrutskie et al. 2006) photometry and astrometry to discover a new nearby late-M dwarf WISE J0720, a relatively bright, red object not far from the Galactic plane ($b = +2.3$ deg; Fig. 1), where confusion has historically been a major obstacle to discovering new nearby, and high proper motion (HPM) objects (i.e., Ivanov et al. 2013).

⋆ Based on observations made with the Southern African Large Telescope (SALT), the DDT Proposal Code 2013-2-RSA-016.
⋆⋆ Senior Research Associate, F.R.S.-FNRS, Belgium.

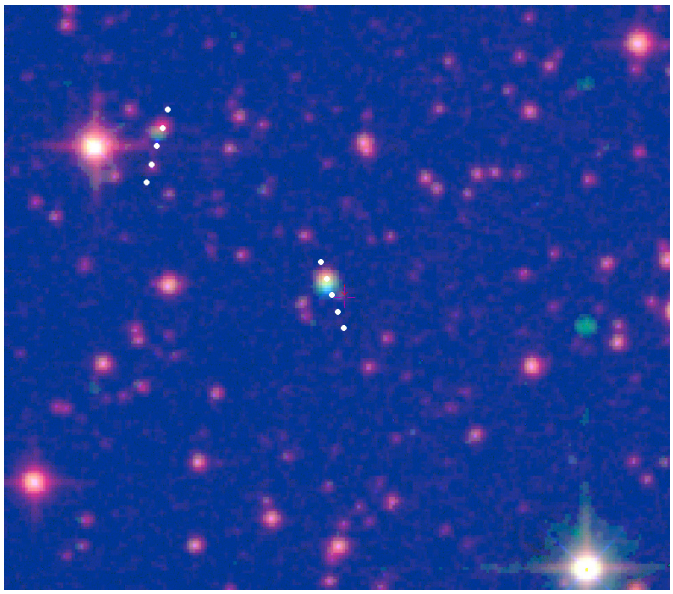

Fig. 1. A false-color composite of DSSII IR (red), 2MASS K_S (green), and our SofI K_S image (blue) with ~3.5 × 3 arcmin field of view, centered at WISE J0720. North is up and east is to the left. Another HPM star 2MASS J07200708−0845589, not related to WISE J0720, is visible to the northeast of WISE J0720. The bright green dots on the western side, with no counterparts in the other images, are cross-talk artifacts in the 2MASS. The white dots show the positions of the two HPM stars in 50 yr steps, over a −50−150 yr period, with respect to the DSS2 IR epoch (see Table 5).

The star is cataloged in USNO B1.0 Monet et al. (2013) with proper motion $\mu_\alpha \cos\delta = -36 \pm 13$, $\mu_\delta = -102 \pm 27$ mas yr^{-1}. Scholz (2014) astrometrically recalibrated the archival images from the previous surveys that had detected WISE J0720, and measured a trigonometric parallax of $\varpi = 142 \pm 38$ mas ($d = 7.0 \pm 1.9$ pc), and a revised proper motion of $\mu_\alpha \cos\delta = -41 \pm 2$, $\mu_\delta = -116 \pm 2$ mas yr^{-1}. The colors of the object were used to estimate a spectral type of M9 ± 1. A comparison of the apparent mid-infrared (MIR) magnitudes of WISE J0720 with some M8-L0 dwarf stars with well-known trigonometric parallax distances suggests a photometric distance in the range 6.0−8.4 pc; a comparison of the IR photometry of the star to the best fit standard (M9V star LP 944-20) hinted at a closer distance of 5.0 ± 1.2 pc. The offset between the latter photometric distance and the trigonometric parallax distance prompted Scholz (2014) to propose that the target may be an unresolved binary. LP 944−20 is considered as young as, perhaps, 0.3 Gyr (Ribas 2003). However, strong doubts about the coevality of its purported moving group (Castor) by Mamajek et al. (2013) suggest that the age of LP 944−20 may not be as well constrained as previously thought. If LP 944−20 is indeed young, or at least younger than WISE J0720, then using it as an M9 template may partially explain the closer photometric distance to WISE J0720.

Here we report comprehensive follow-up observations of WISE J0720 aimed at constraining its physical parameters.

2. Observations

2.1. Optical spectroscopy

We obtained long-slit spectra of WISE J0720 with the Robert Stobie Spectrograph (RSS; Burgh et al. 2003; Kobulnicky et al. 2003) at the Southern African Large Telescope (SALT; Buckley et al. 2006; O'Donoghue et al. 2006) in Sutherland, South Africa on 2013-Nov-13/14. Two spectroscopic setups were used, both with a 0.6 arcsec wide slit at a parallactic angle (PA = −137.3 deg) and with an on-chip 2 × 2 binning giving a spatial scale of 0.253 arcsec pix^{-1}. The higher resolution spectrum using the PG1800 grating results in the spectral coverage of $\lambda \sim 7840$–9000 Å and a resolution of 0.97 Å (0.33 Å per binned pixel), while the lower resolution setup using the PG0900 grating provided 2.19 Å (1.89 Å per binned pixel) resolution over $\lambda \sim 6300$–9000 Å range. A 900 s exposure was used for the former, and a 1060 s exposure for the latter. The seeing during both observations was 1.8 arcsec. A neon lamp arc spectrum and a set of calibration flats were taken immediately after the science frames. A spectrophotometric standard star, HR 9087, was observed for both setups.

The data were reduced following the same procedure as in Kniazev et al. (2013). The SALT data pipeline PySALT (Crawford et al. 2010) products were used for primary reductions including the overscan, gain, cross-talk corrections, and mosaicing. Additional routines in MIDAS[1] (Banse et al. 1983, 1988; Warmels 1992) and in the *twodspec* package in IRAF[2] were used for wavelength calibration, frame rectification, and background subtraction of the 2D spectrum (Kniazev et al. 2008). The red part (>8000 Å) of the spectra suffers from significant fringing effects, which are mitigated by using the calibration flats. The wavelength calibration for PG1800 and PG900 gratings resulted in an internal uncertainty of $\sigma = 0.03$ Å and $\sigma = 0.13$ Å respectively. The spectrophotometric standard was used for the spectral shape calibration, but no attempt was made to correct for slit losses or the changing pupil size of SALT. The velocities were corrected for heliocentric motion. The 1D spectra were extracted using a 5 pixel, ~1.3 arcsec, aperture. The final spectra are shown in Fig. 2 (left).

We measured equivalent widths of some of the more prominent features in our spectra with the IRAF task splot. The results are listed in Table 1. The errors reflect the uncertain continuum, and they are determined as the r.m.s. of multiple measurements. The Li I line at $\lambda = 6707$ Å was not detected, and we only give a 1σ limit. The flux of the H_α emission line was $7.6 \pm 0.2 \times 10^{-16}$ erg cm^{-2} s^{-1}. This error, however, does not include uncertainties of absolute flux calibration due to slit losses, which can easily amount to a factor of a few, as the comparison of the optical and the near-infrared (NIR) spectra in Fig. 2 suggests.

The spectral indices of Kirkpatrick et al. (1999) were also measured because of their utility for spectral typing. The results are listed in Table 2. The typical discrepancies between indices derived from the lower and the higher resolution spectra are 0.02–0.05, suggesting errors on that order of magnitude.

A radial velocity $V_{obs} = 53.79 \pm 2.54$ km s^{-1} was measured from the higher resolution spectrum (taken at UT = 00:42), using the absorption lines at $\lambda = 7947.60$, 8521.13, 8183.255, and 8194.790 Å. The measurement of each line was verified with the nearest night sky lines using the method and programs described in Zasov et al. (2000). The barycentric correction was 22.77 km s^{-1}, and the final heliocentric velocity was calculated to be $V_{hel} = 76.56 \pm 2.54$ km s^{-1}. The final heliocentric velocity using the Hα emission line from the spectrum obtained with the PG900 grating was $V_{hel} = 77.65 \pm 3.79$ km s^{-1}, fully consistent with the higher resolution spectrum.

[1] Munich Image Data Analysis System is distributed by ESO.
[2] IRAF is distributed by the NOAO, which is operated by the AURA under cooperative agreement with the NSF.

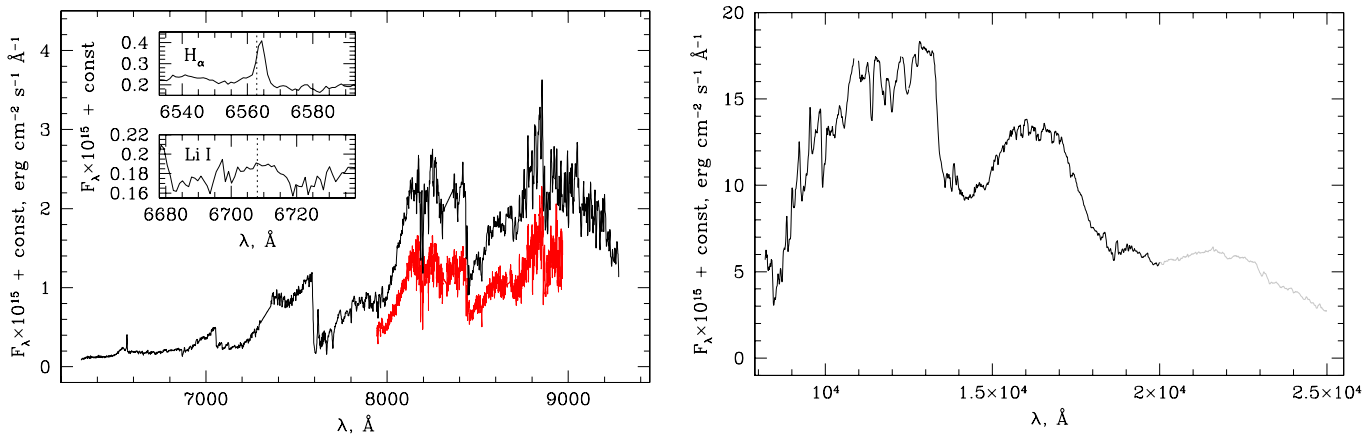

Fig. 2. Optical (*left*) and NIR (*right*) spectra of WISE J0720. The low-resolution optical spectrum is plotted in black, the medium-resolution in red. The reddest part of the NIR spectrum, affected by a wavelength calibration problem (see Sect. 2.2 for details) is shown in gray. The gap at ∼11 000 Å is an omitted cosmic ray hit. The insets on the left zoom in on the regions around the Hα and the Li I features, and the dotted vertical lines show their rest-frame positions. The mismatch between the fluxes of the three spectra are probably due to unaccounted for slit losses.

Table 1. Equivalent widths for the more prominent spectral features of WISE J0720 in angstroms.

Feature, λ	Value	Feature, λ	Value	Feature, λ	Value
Optical features:					
Hα 6563	−3.9 ± 0.1	Rb I 7800	1.6 ± 0.1	Sc I 8520	0.5 ± 0.1
Li I 6707	≤0.07	Rb I 7948	1.1 ± 0.1		
Near-infrared features:					
Na I 11380	7.2 ± 0.5	K I 12432	6.5 ± 0.3	Na I 22062	6.5 ± 0.7
Na I 11400	6.8 ± 0.3	K I 12527	6.7 ± 0.9	Ca I 22640	0.9 ± 0.2
K I+Fe I 11690	6.4 ± 0.2	K I 15168	3.6 ± 0.2		
K I 11780	9.6 ± 0.4	Mg I 15025	1.7 ± 0.9		

Notes. The line wavelengths λ are listed in Å.

Table 2. Spectral indices for WISE J0720, defined by Kirkpatrick et al. (1999), and measured on our SALT spectra (the grating setup is given in brackets).

Index	Value	Sp. type	Index	Value	Sp. type
Rb-a	1.15 (GR900)	M7–L0	Cs-b	1.16 (GR1800)	L2–L4
Rb-b	1.25 (GR1800)	L0–L2	Cs-b	1.12 (GR900)	L0–L3
Rb-b	1.15 (GR900)	M7–L0	TiO-a	1.82 (GR900)	M9-L0
Na-a	1.20 (GR1800)	M9–L2	TiO-b	1.82 (GR1800)	M9-L1
Na-a	1.19 (GR900)	M9–L2	TiO-b	1.85 (GR900)	M9-L1
Na-b	1.35 (GR1800)	M7–L0	CrH-b	1.04 (GR1800)	M8-L2
Na-b	1.33 (GR900)	M7–L0	CrH-b	1.01 (GR900)	M8-L2
Cs-a	1.18 (GR1800)	L1–L3	FeH-a	1.12 (GR1800)	M7-9
Cs-a	1.20 (GR900)	L1–L3	FeH-a	1.12 (GR900)	M7-9

Notes. The derived spectral types from the spectral sequences in Kirkpatrick et al. (1999; Figs. 8–10) are listed.

2.2. Near-infrared spectroscopy

Low-resolution long-slit NIR spectroscopy of WISE J0720 was carried out on 2013-Nov-16/17, with the Folded-Port InfraRed Echellette spectrograph (FIRE; Simcoe et al. 2008; Simkoe et al. 2013) at the *Magellan* telescope at Las Campanas Observatory. The instrument is equipped with a 2048 × 2048 HAWAII-2RG detector. We obtained four 1 s exposures in ABBA nodding pattern in the high-throughput prism mode, covering λ = 0.82–2.51 μm. The slit was 1 arcsec wide, and the spatial scale was 0.15 arcsec px^{-1}. The spectral resolution varies from $R \sim 500$ in the J atmospheric window, to ∼300 in the K window. An A0V telluric HD 65504 was observed to correct for the atmospheric absorption.

Table 3. Spectral indices for WISE J0720, defined by McLean et al. (2003) and measured on our low-resolution FIRE spectrum.

Index	Value	Sp. type	Index	Value	Sp. type
H_2OA	0.66 ± 0.01	L1 ± 1.5	H_2OD	1.02 ± 0.01	M9 ± 1
H_2OB	0.77 ± 0.01	L2 ± 1	J−FeH	0.90 ± 0.01	M8 ± 2
H_2OC	0.68 ± 0.01	L2 ± 2	z−FeH	0.76 ± 0.04	M7 ± 2

Notes. The derived spectral types from the spectral sequences in McLean et al. (2003) are listed. The methane indices were omitted, because they cannot constrain the spectral type of M- or L-type objects, and the CO index was omitted because it is in an unreliable part of the spectrum.

The data reduction performed was typical for the NIR spectra (e.g., Ivanov et al. 2000, 2004): sky subtraction, tracing and extraction of 1D spectra, wavelength calibration with neon-argon lamp spectra taken right after the target observation, combination of the 1D spectra in wavelength space, and telluric correction. We also multiplied the spectra by an A0 spectrum from the library of Pickles (1998) to remove the artificial features, introduced by the telluric itself. At this low resolution the arc lines above ∼20 000 Å were blended, affecting the wavelength calibration. Probably, the best way to treat this issue is to take two arcs, one with a narrow slit and another with a wide slit, derive a wavelength calibration from the former, and then to apply a shift to the latter using the lines in the wide slit arc that are not blended. This problem resulted in smearing of the spectra in the K band, so we did not use this part of the spectra in the subsequent analysis. The spectrum was pseudo-flux calibrated to the apparent 2MASS H band magnitude. The other bands were not used because J transmission is known to depend on the water vapor, and the K spectrum not reliable, as pointed out above. The final spectrum is shown in Fig. 2 (right).

We measured the indices defined in McLean et al. (2003) because of their common use (Cushing et al. 2005) and straightforward parametrization versus spectral class over M- and L-type objects. The results are listed in Table 3. The errors reflect only the formal uncertainties in the wavelength calibration, and were determined by by varying the position of the pass bands.

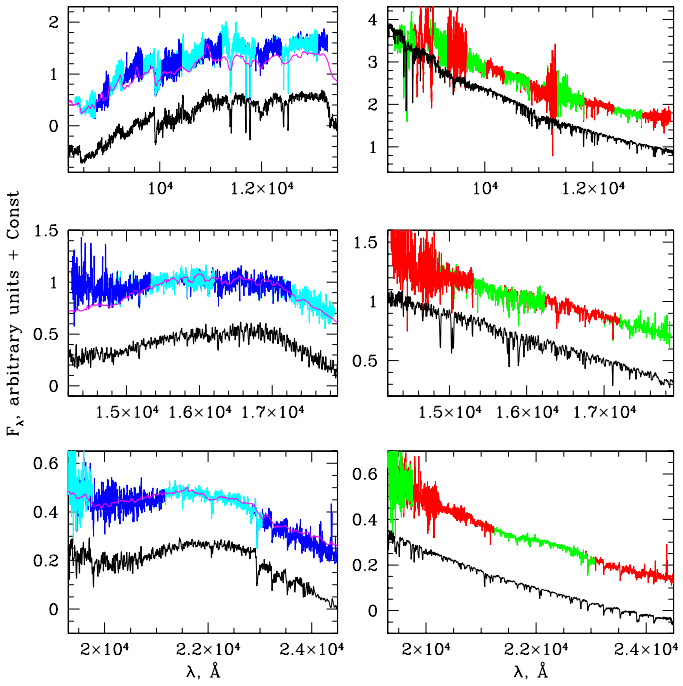

Fig. 3. Medium-resolution NIR spectra of WISE J0720 (*left*) and the radial velocity standard HD 48381 (*right*). The different orders are plotted with alternating dark/light blue and red/green colors, respectively. The low-resolution NIR spectrum of WISE J0720 is shown in magenta. For comparison we plot the M9V LP 944−20 (*left*, black) and K0V HD 145675 (*right*, black) spectra from the IRTF library (Cushing et al. 2005; Rayner et al. 2009), shifted down by 0.9 (*top panels*), 0.5 (*middle*) and 0.3 (*bottom*). All spectra were normalized to unity for λ between 15 000 Å and 17 000 Å.

A medium-resolution NIR spectrum of WISE J0720 was collected on 2013-Nov-18/19, with the same instrument. We obtained four 120 s exposures in ABBA nodding pattern in Echelle mode, covering a similar range to the one above. The slit was 0.6 arcsec wide. The spectral resolution, measured from ThAr lines, was $R \sim 5000$. The A0V telluric star HD 65504 was observed in order to correct for atmospheric absorption. We also obtained spectra of a K0IV radial velocity standard HD 48381 ($V_{\rm helio}$ = 40.722 km s^{-1}, ±0.0065 internal error, ±0.0145 rms of 16 measurements; Soubiran et al. 2013), and a corresponding A0 telluric star HIP 32479.

Each of the 21 orders was treated separately, and the reduction steps were the same as for the low-resolution data. We used ThAr lamp spectra taken for the wavelength calibration of the eight bluest orders, and sky lines for the remaining thirteen. The final spectra are shown in Fig. 3. The global shapes of the low- and the medium-resolution NIR spectra do not match particularly well for $\lambda < 15\,000$ Å. A number of factors can account for this, including a change of the atmospheric transmission between the observation of the target and the telluric calibrator, and error in the spectral type of the telluric or wavelength dependent slit losses. The two spectra appear similar at $\lambda > 20\,000$ Å, however, despite the wavelength calibration problem mentioned above.

We measured the equivalent widths of some prominent features in the NIR spectrum, following the same procedure as for the optical spectra. The results are listed in Table 1.

We used the IRAF task *fxcor* to measure the velocity difference between WISE J0720 and HD 48381 with the CO band heads. They appear in two separate orders, so we obtained two independent measurements: $\Delta V_{\rm obs}$ = 50.4 ± 13.8 and 53.8 ± 20.1 km s^{-1}. Throughout this paper we adopt their weighted average $\Delta V_{\rm obs}$ = 51.8 ± 12.0 km s^{-1}. The heliocentric correction for the radial velocity standard at the moment of the observation (UT = 08:10) was −12.4 km s^{-1}, yielding an observed radial velocity of 28.3 km s^{-1}. Adding the measured difference we obtain an observed velocity of the target of 81.1 km s^{-1}. The heliocentric correction for the target at the moment of the observation (UT = 07:41) was 21.4 km s^{-1}, so the heliocentric radial velocity of the target was $V_{\rm hel}$ = 101.6 ± 12.0 km s^{-1} (the implications of this measurement will be discussed in Sect. 3.1).

Finally, we tested the consistency of these results measuring the relative velocity difference of the CO band heads in the two orders, obtaining 11.0 ± 7.9 km s^{-1} for the target, and 14.6 ± 10.3 km s^{-1} for the standard, respectively. The difference is below the measurement errors.

Table 4. Apparent magnitudes of WISE J0720 in the Vega system and calibration coefficients.

Band	Zero point	c_1	c_2	Color	Apparent mag
B	25.182 ± 0.103	0.06	0.0330	$B-V$	20.778 ± 0.140
V	25.457 ± 0.051	0.05	0.0730	$B-V$	18.266 ± 0.096
R	25.648 ± 0.029	0.04	0.0056	$V-R$	15.838 ± 0.031
i	24.901 ± 0.035	0.00	0.0760	$R-i$	14.019 ± 0.035
CMC15 r					16.850± –
DENIS I					13.805 ± 0.02
DENIS J					10.674 ± 0.06
DENIS K_S					9.399 ± 0.09
2MASS J					10.628 ± 0.023
2MASS H					9.919 ± 0.024
2MASS K_S					9.467 ± 0.019
WISE $W1$					9.174 ± 0.023
WISE $W2$					8.860 ± 0.022
WISE $W3$					8.333 ± 0.024
WISE $W4$					7.934 ± 0.212

Notes. NIR magnitudes were not derived because the core of the target was registered in the nonlinear regime of the detector. We also list the literature data used for the spectral energy distribution fit: The Carlsberg survey (Evans et al. 2002, release 15; SDSS r filter), DENIS (Epchtein et al. 1997), 2MASS (Skrutskie et al. 2006), and WISE (Wright et al. 2010).

2.3. Optical imaging

Optical *BVRi* images of WISE J0720 were obtained with EFOSC2 (Buzzoni et al. 1984; Snodgrass et al. 2008) at the ESO New Technology Telescope on 2013-Nov-15/16. It is equipped with a 2048 × 2048 Loral/Lesser CCD, delivering 0.12 arcsec px^{-1} images over a ∼4.1 × 4.1 arcmin field. The following exposures were taken: 30, 20, 10, and 2 s in *BVRi* with 2 × 2 binning for photometry and ten 2 s images in i with 2 × 2 binning for astrometry.

The data reduction included bias subtraction and flat fielding. The photometric calibration was based on *BVRi* observations of two standards: PG 2213−006 and RU 152. The magnitudes in the standard system $m_{\rm std}$ were calculated as

$$m_{\rm std} = {\rm ZP} + m_{\rm inst} + 2.5 \times \log_{10}(t) + c_1 \times sec\, z + c_2 \times {\rm color} \quad (1)$$

where ZP was the zero point, $m_{\rm inst}$ was the magnitude in the instrumental system, c_1 was the extinction coefficient (adopted from historic La Silla records), c_2 was the color coefficient; the values of the coefficients and the colors used in the color terms for each band are listed in Table 4.

2.4. Near-infrared imaging

Near-infrared JHK_S images of WISE J0720 were obtained with SofI (Moorwood et al. 1998) at the ESO New Technology Telescope on 2013-Nov-13/14. The instrument is equipped with a 1024 × 1024 Hawaii HgCdTe detector, delivering 0.29 arcsec px^{-1} images over a ∼4.9 × 4.9 arcmin field. Four jittered images were taken in each filter, and each image was the average of five 2 s frames in J, and five 1.182 s frames in H and K_S, the total integration times in the three NIR bands are 40, 23.64, and 23.64 s, respectively. The core of the object is at the nonlinear regime even at the shortest detector integration time, so these images are used only for astrometry of the target, and to search for fainter nearby companions, particularly when future high angular resolution observations become available.

The data reduction includes the usual steps: flat fielding, sky subtraction, image alignment, and combination. The photometric calibration is based on isolated non-saturated 2MASS stars in the field, spanning $J - K_S \sim 0.3–1.0$ mag range. The zero points (listed in Table 4) were derived from 18, 15, and 19 stars, respectively for J, H, and K_S. No significant color terms were found.

The astrometric calibration was based on all stars in the field, and yields the following position: $\alpha = +108.7242$ deg = 07:14:53.8, $\delta = -8.780546$ deg = −08:46:49.97 (J2000), with positional errors of 0.1 arcsec. A false-color composite of DSSII IR, 2MASS K_S, and our SofI K_S image is shown in Fig. 1.

2.5. X-ray observations

The *Swift* satellite (Gehrels et al. 2004) observed the field of WISE J0720 on 2004-Jun-04, starting at UT = 21:35. A full band X-ray Telescope (XRT) image was extracted (in Photon counting mode, OBSID=00049016001, and exposure time 529 s) from the UK Swift Science Data Centre, which is a pre-reduced product using standard procedures.

With only one source count being detected over the full energy range around the position of WISE J0720, the object is undetected in X-rays. The 3σ uncertainty on the count rate is 5.7×10^{-3} ct s^{-1}. Assuming an optically-thin thermal plasma with temperature $kT = 0.3$ keV (e.g., Tsuboi et al. 2003) implies a 0.3–2 keV flux limit of 1.2×10^{-13} erg s^{-1} cm^{-2}, or X-ray luminosity upper-limit of $5.3(\pm2.9) \times 10^{26}$ erg s^{-1} for a distance of 6.07 pc (see Sect. 3.1). The column density of obscuring gas along the line of sight to the source is assumed to be negligible, given the proximity of WISE J0720.

The spectral energy distribution (SED) fit of WISE J0720 (Sect. 3.3) predicts a bolometric luminosity of 2.02×10^{-4} $L_\odot$, yielding $\log(L_X/L_{bol}) \leq -3.2$. This luminosity constraint is weaker than those available for other well-studied late-type dwarfs, and much weaker than for the nearest known brown dwarf (BD) Luhman-16 (Gandhi et al. 2013). It lies close to the level of saturated emission, $\log(L_X/L_{bol}) = -3$, expected for the M9 spectral class (Berger et al. 2010).

3. Results

3.1. Kinematics of WISE J0720

Weight-averaging the optical and the NIR heliocentric velocities ($V_{hel} = 76.56 \pm 2.54$ and 101.6 ± 12.0 km s^{-1}, respectively), we obtain 77.6 ± 2.5 km s^{-1}. Combining our new position of WISE J0720 with the previous ones reported by Scholz (2014), we obtain improved proper motions of $\mu_\alpha \cos\delta = -39.1 \pm 2.1$ $\mu_\delta = -111.8 \pm 1.9$ mas yr^{-1} and a parallax distance of 6.07 pc, with a 1σ interval between 5.12 pc and 7.43 pc. The transverse velocity is $V_{tan} = 3.4 \pm 0.1$ km s^{-1}.

We calculate the barycentric velocity of WISE J0720 on the Galactic coordinate system using the proper motion and parallax from Scholz (2014), and our optical radial velocity (because of the smaller uncertainty): $(U, V, W) = -63.7 \pm 2.1$, -65.4 ± 1.4, 0.6 ± 1.1 km s^{-1}. The total barycentric speed is $S = 91.4 \pm 1.8$ km s^{-1}. Adopting the local standard of rest (LSR) from Schönrich et al. (2010), the velocity translates to LSR velocity $(U_{LSR}, V_{LSR}, W_{LSR}) = -52.6, -53.2, 7.8$ km s^{-1}, and total LSR peculiar motion of 75.2 km s^{-1}. We estimate kinematic membership probabilities of 65.1%, 34.6%, and 0.3% to the thin disk, thick disk, and halo, respectively, using the velocity moments and the local density normalizations of the these dominant Galactic kinematic populations from Bensby et al. (2003), and adopting the LSR velocity from Schönrich et al. (2010). Given the large LSR velocity (75 km s^{-1}), and the probabilities calculated above, it seems most likely that WISE J0720 is either an old thin disk or a thick disk star. Comparing the velocity of WISE J0720 to field F and G dwarfs in Fig. 1 of Bensby et al. (2007) shows that it is in the velocity region overlapping thin and thick disk stars, and that if it belongs to the thin disk, it could be associated with the Hercules dynamical stream (U_{LSR}, $V_{LSR} \approx -40, -50$ km s^{-1}), which unfortunately is of negligible help in constraining its age. Using an epicycle orbit code[3] we estimate that the Galactic orbit of WISE J0720 has perigalacticon $R_p \simeq 3.27$ kpc and apogalacticon $R_a \simeq 8.44$ kpc, and that it is highly eccentric: $e \simeq 0.44$.

A search of the XHIP catalog (Anderson & Francis 2012) finds only one Hipparcos star with velocity within 4 km s^{-1} of WISE J0720 – HIP 96426, a slightly supersolar ([Fe/H] = 0.08; Boeche et al. 2011) K dwarf at $d \simeq 46 \pm 4$ pc – and although it shares the velocity of WISE J0720, it is too distant to be considered as a physical companion.

3.2. Spectral typing

A comparison of the overall shape of our optical spectra with templates from the Dwarf Archives[4] (Henry & Kirkpatrick 1990; Kirkpatrick et al. 1995, 1999, 2000; Kirkpatrick 2003; Gelino et al. 2004) suggest a spectral type of M8.5–M9 (Fig. 4), consistent with the estimate of Scholz (2014).

We also estimated the spectral type of WISE J0720 from the spectral indices defined by Kirkpatrick et al. (2011) and McLean et al. (2003), listed in Tables 2 and 3, using as reference the sets of measurements published in these papers. The optical indices proved to be of limited use because of the considerable scatter and the non-monotonic behavior of some indices near the M/L transition. The NIR CO index was omitted from this analysis, because it shows nearly constant strength in the range of spectral types of interest. The two methane indices yield limits because this feature only gains strength in extremely cool objects, later than L8 type.

The Hα equivalent width (Table 1) places WISE J0720 in the regime of the quiescent late M-type field dwarfs (Mohanty & Basri 2003). The lack of Li I absorption makes it a likely main-sequence star or a relatively old massive

[3] We follow the epicycle equations of Fuchs et al. (2006), and adopt Oort A and B parameters from Feast & Whitelock (1997), local disk density from (van Leeuwen 2007), LSR velocity from Schönrich et al. (2010), solar Galactocentric radius 8.0 kpc, and solar distance above Galactic plane of 20 pc.

[4] dwarfarchives.org/

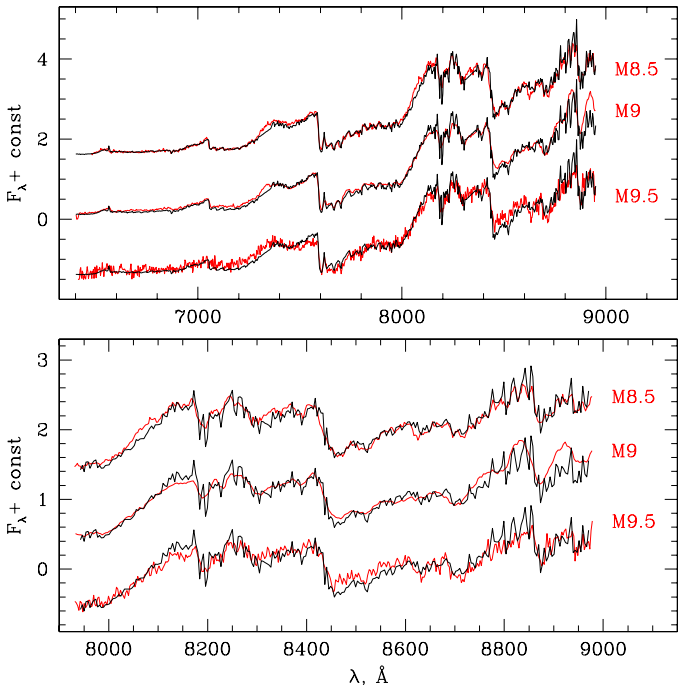

Fig. 4. Low-resolution (*top*) and medium-resolution (*bottom*) optical spectra of WISE J0720 (black) compared with template spectra from the Dwarf Archives (red; Henry & Kirkpatrick 1990; Kirkpatrick et al. 1995, 1999, 2000; Kirkpatrick 2003; Gelino et al. 2004). Our spectra were re-binned by factors of 4 (*top panel*) and 12 (*bottom panel*) for display purposes.

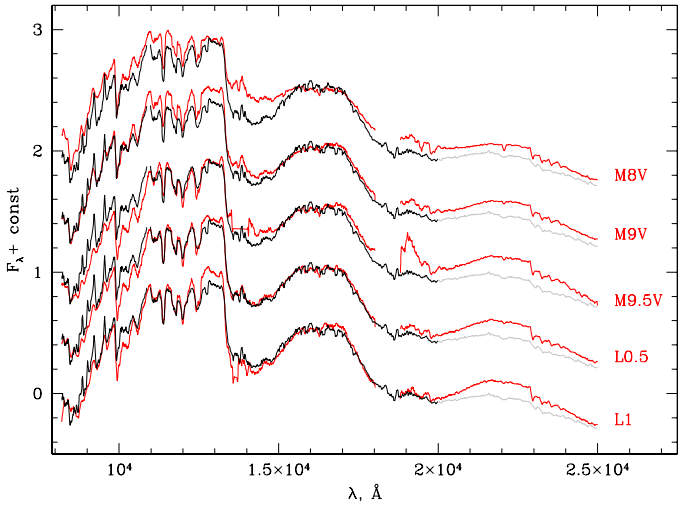

Fig. 5. NIR spectrum of WISE J0720 (black; gray for the region with $\lambda \geq 20\,000$ Å that is not used for spectral typing because of the poor wavelength calibration, see Sect. 2.2) compared with templates from the IRTF library (red; Cushing et al. 2005; Rayner et al. 2009). As in Fig. 2, the cosmic ray hit region is omitted.

BD (>0.055 $M_\odot$; e.g., Burrows et al. 1997; Baraffe et al. 1998) that has exhausted its lithium supply.

The overall appearance of our low resolution NIR spectrum resembles the spectra of objects at the M-L transition (Fig. 5; ignore the problematic red part, as discussed in Sect. 2.2). Finally, our medium resolution NIR spectrum shows no Al I doublet at $\lambda = 16\,724/16\,756$ Å. This feature is still discernible in M9 stars (Cushing et al. 2005, Figs. 8, 9), indicating an early L-type for WISE J0720.

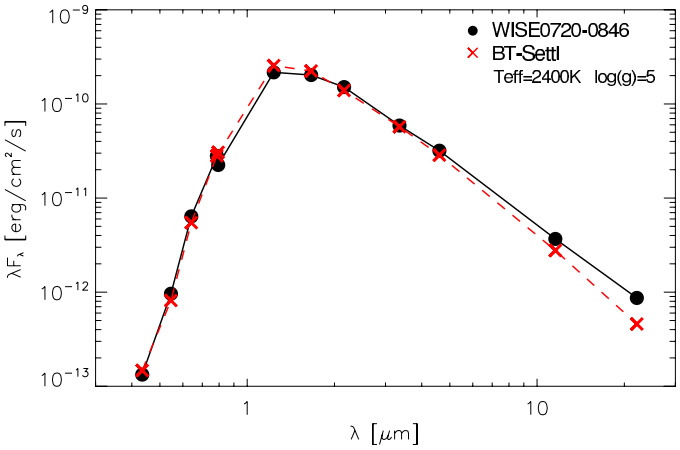

Fig. 6. SED fitting of WISE J0720. The black dots show the photometric measurements listed in Table 4. The uncertainties are comparable to or smaller than the size of the symbols. For details see Sect. 3.3.

In summary, the optical spectra yield a range of types from M7 to L4, the most probable being M9, while the NIR spectra suggest an early L. Therefore, we assign to WISE J0720 a spectral type of L0 (with a tentative uncertainty of one subtype), which is in the middle of the range of values, determined from all available data, with a variety of methods. There may be some discrepancy between the optical and the NIR spectra, but we do not consider it significant enough to suggest a composite M/L spectrum.

3.3. Spectral energy distribution fitting

The SED of WISE J0720, along with the best-fit BT-Settl (Allard et al. 2011) model is shown in Fig. 6, and magnitudes used are listed in Table 5. A χ^2 minimization was performed with VOSA (Virtual Observatory SED Analyzer; Bayo et al. 2008), on a grid of BT-Settl models with effective temperature $T_{\rm eff}$ between 2000 K and 4000 K, surface gravity $\log g$ between 2 dex and 6 dex, and metallicity [M/H] between −4 and 0.5. The best fit corresponds to $T_{\rm eff} = 2400$ K, $\log g = 4.5$, and [M/H] = 0, and it is plotted with red crosses. The uncertainties in $T_{\rm eff}$ and metallicity are 100 K and 0.5 dex, reflecting the spacing of the model grid. The VOSA also finds matching dusty isochrones for the best SED fit yielding ages from 0.5 Gyr to 1.0 Gyr and a mass of 0.06−0.08 $M_\odot$.

The apparent excess at the WISE 12 and 22 μm bands could not be accounted for with lower $\log g$ and $T_{\rm eff}$; to obtain a satisfactory fit in the MIR, $T_{\rm eff} \sim 2000$ K is required, but this would predict fluxes that are too low in the optical pass bands. If real, this excess would hint at the presence of a disk, or at an unresolved cooler companion. The disk is unlikely given the probable old age of WISE J0720. To test the ability of VOSA to match the properties of cool objects we also tried fitting LP 944−20, the M9 object used by Scholz (2014) as a template. The best fit with BT-Settl models for $\log g = 5$ yields $T_{\rm eff} = 2400$ K, and [M/H] = 0, leaving again some excess in the WISE bands. The excess disappears if $\log g = 2$−3, hinting that LP 944−20 may indeed be a younger object than WISE J0720, as discussed in Sect. 1.

3.4. Binarity and a search for wide co-moving companions

Scholz (2014) argued that WISE J0720 may be a binary because it appeared brighter for its spectral type and the parallactic distance he determined. Some of our data do not support

this possibility: our improved parallax suggests a distance of $6.07^{+1.36}_{-0.95}$ pc, in agreement with the apparent brightness of the object, rejecting the possibility for nearly equal mass companions; a high mass ratio binary can yield conflicting spectral types in the optical and in the NIR, which is not the case here; a white dwarf companion is made unlikely by our *BV* band imaging and SED fitting, as a simple comparison with Sirius B shows; the K_S imaging taken under 0.6 arcsec seeing failed to resolve WISE J0720 into a wide binary.

This leaves the possibility that it is a tight unresolved binary, and the difference between the radial velocity derived from the optical and NIR spectra seem to support this option. The secondary needs to be massive enough. i.e., a BD, on a close-in orbit, so it can generate a radial velocity amplitude of ≥25 km s^{-1} within only three days. However, the formal significance of this difference is at the 2σ level, and the two spectra were obtained with different instruments that are not designed for accurate radial velocity monitoring. The disagreement may be due to some hidden systematic effects. The question whether WISE J0720 is a tight binary will need additional observations at higher spectral resolution.

We searched for wide co-moving companions to WISE J0720 by visually inspecting 6×6 arcmin false-color images created from archival images of the region around WISE J0720 and our NIR images. The motion of WISE J0720 was clearly discernible (Fig. 1). The sensitivity of the search was determined by the depth and the angular resolution of the shallowest image or the image with the worst image quality. The most stringent constraints come from the 2MASS–SofI comparison: the seeing on the 2MASS images was 2−2.5 arcsec (to be compared with 0.5–0.6 arcsec on our NIR images); the nominal 2MASS completeness limits, determined from the luminosity function downturn, for JHK_S, are ∼15.8, 15.1, and 14.3 mag, respectively (Skrutskie et al. 2006).

Down to those limits we found no co-moving companions of WISE J0720, but we rediscovered another relatively bright (K_S = 12.8 mag) HPM star 2MASS J07200708−0845589 (Table 5). The PPMXL Catalog (Roeser et al. 2010) reports $\mu_\alpha \cos\delta$ = 92.7 ± 7.4, μ_δ = −167.8 ± 7.4 mas yr^{-1}. Adding the positions from WISE and SofI, we obtain $\mu_\alpha \cos\delta$ = 37.0 ± 3.8 mas yr^{-1} and μ_δ = −124.2 ± 0.79 mas yr^{-1} with a rather large χ^2 = 356 which is probably due to discrepant WISE and SofI positions, probably indicating a different degree of background contamination in the NIR and MIR regimes. The parallax is also poorly constrained; we find V_{tan} = 102 ± 39 mas, indicating a distance d ∼ 10 pc. The VOSA SED fit with the BT-Settl models to CMC15 *r*, DENIS IJK_S, 2MASS JHK_S, and WISE W1 to W3 measurements yielded T_{eff} = 3500 K, $\log g$ = 6, and [M/H] = −1. The grid spanned the ranges of 2000−4500 K, 2–6, and −2.5–0, respectively. Weak excess is visible at *W*3, but as for WISE J0720, we are reluctant to claim the presence of a disk or a faint companion. There is X-ray source 1RXS J072007.6−084541 at 20 arcsec separation, but Haakonsen & Rutledge (2009) associate it, albeit with low probability for a unique association of 0.374, with another object, namely 2MASS J07200855−0846031.

4. Summary and conclusions

We carried out a comprehensive follow-up observation of WISE J0720, an L0 object at ∼5−8 pc from the Sun, reported by Scholz (2014). New NIR imaging allows us to redetermine the distance to WISE J0720, reducing it to $6.07^{+1.36}_{-0.95}$ pc, bringing into agreement the geometric and the photometric distances. A binary nature of WISE J0720 was considered by Scholz (2014) because the object appeared brighter for its spectral type and parallactic distance.

Our spectroscopic observations yield spectral type L0 ± 1, close to the M9 determined by Scholz (2014). WISE J0720 is the third closest L dwarf to the Sun, after DENIS-P J025503.3−470049 (Table 4 in Kirkpatrick et al. 2012) and the recently discovered WISE J104915.57-531906.1A by Luhman (2013). For the first time we measure the heliocentric radial velocity of WISE J0720, obtaining 76.56 ± 2.54 and 101.6 ± 12.0 km s^{-1} from the optical and the NIR spectra, respectively (obtained three days apart). They agree at the 2σ level, and cannot be considered evidence for the presence of a close-in companion. The weighted average heliocentric velocity is V_{hel} = 77.6 ± 2.5 km s^{-1}. Combined with the proper motions, this yields Galactic velocities that make the object a likely member of the disk or the thick disk. It is not associated with any of the known nearby young moving groups. WISE J0720 shows weak Hα emission, consistent with the modest chromospheric activity of field M and L dwarfs. The optical spectra show no detectable Li I, suggesting that the object is massive enough to have processed its primordial lithium content.

We also report new *BVRi* imaging, and use it, together with the literature magnitudes to constrain the SED of WISE J0720, yielding T_{eff} ∼ 2400 K, consistent with the determined spectral type. We also note a weak excess at $\lambda > 10$ μm, but consider it to be a problem of the models rather than reliable evidence for the presence of a disk or a faint red companion. Adaptive optics observations or high-precision radial velocity monitoring are needed to address these possibilities.

Finally, a HPM star, 2MASS J07200708−0845589 was rediscovered serendipitously in the field of WISE J0720, and we report improved PMs for this object.

During the refereeing process we became aware of the work of (Burgasser et al. 2014), who obtained M9.5 spectral type for WISE J0720, and measured radial velocity of 83.8 ± 0.3 km s^{-1} and distance of 6.0 ± 1.0 pc, in agreement with our results within

Table 5. Coordinates of a HPM star 2MASS J07200708−0845589 in the vicinity of WISE J0720.

Image	RA, Dec (J2000)	Epoch, UT yyyy-mon-dd hh:mm:ss
DSS1 Blue	07:20:06.986−08:45:53.13	1955-Nov-19 11:38:00
DSS1 Red	07:20:06.995−08:45:52.89	1955-Nov-19 10:43:00
DSS2 IR	07:20:07.012−08:45:56.06	1981-Mar-11 11:03:00
DSS2 Blue	07:20:07.012−08:45:56.78	1982-Dec-11 16:44:00
DSS2 Red	07:20:07.044−08:45:57.43	1985-Dec-15 15:51:00
2MASS *J*	07:20:07.086−08:45:59.02	1999-Feb-21 01:27:32
2MASS *H*	07:20:07.085−08:45:59.17	1999-Feb-21 01:27:32
2MASS K_S	07:20:07.089−08:45:59.11	1999-Feb-21 01:27:32
WISE *W*1	07:20:07.108−08:46:00.88	2010-Apr-10 00:15:12
WISE *W*2	07:20:07.098−08:46:00.88	2010-Apr-10 00:15:12
WISE *W*3	07:20:07.072−08:46:01.02	2010-Apr-10 00:15:12
SofI *J*	07:20:07.130−08:46:00.73	2013-Nov-14 08:20:41
SofI K_S	07:20:07.130−08:46:00.93	2013-Nov-14 08:24:44
SofI *H*	07:20:07.136−08:46:00.92	2013-Nov-14 08:26:08

Notes. It is heavily contaminated on the WISE images by a bright neighbor, and the reddest channel is omitted because it is not useful for a position measurement. The uncertainties are 0.45 arcsec for DSS1, 0.33 arcsec for DSS2 Red and IR, and 0.59 arcsec for DSS2 Blue (Mickaelian 2004), 0.06 arcsec for 2MASS (Skrutskie et al. 2006), 0.15 arcsec for WISE (Wright et al. 2010), and 0.015/0.010 arcsec for SofI, along RA/Dec, respectively.

the uncertainties. Their adaptive optics assisted NIR imaging revealed a faint ($\Delta H \sim 4.1$ mag) T5 BD companion candidate at 0.14 arcsec (~0.8 AU) separation that is undetectable in our data.

Acknowledgements. Some observations reported in this paper were obtained with the Southern African Large Telescope (SALT). Some observations reported in this paper were obtained with the ESO New Technology Telescope under program 60.A-9700. All SAAO and SALT co-authors acknowledge the support from the National Research Foundation (NRF) of South Africa. We acknowledge support from the FONDAP Center for Astrophysics 15010003; BASAL CATA Center for Astrophysics and Associated Technologies PFB-06; the Ministry for the Economy, Development, and Tourisms Programa Inicativa Cientifica Milenio through grant IC 12009, awarded to The Millennium Institute of Astrophysics (MAS); FONDECYT grants No. 1090213, 1130196, and 1110326 from CONICYT, and the European Southern Observatory. J.C.B. acknowledge support from a Ph.D. Fellowship from CONICYT. R.K. acknowledges partial support from FONDECYT through grant 1130140. J.B. acknowledges support from FONDECYT No. 1120601; P.G. thanks STFC for support (grant reference ST/J003697/1). We have also made extensive use of the SIMBAD Database at CDS Strasbourg, of the 2MASS, which is a joint project of the University of Massachusetts and IPAC/CALTECH, funded by NASA and NSF, and of the VizieR catalogue access tool, CDS, Strasbourg, France. Based on data from CMC15 Data Access Service at CAB (INTA-CSIC). We thanks the anonymous referee for suggestions that helped to improve the paper.

References

Allard, F., Homeier, D., & Freytag, B. 2011, in 16th Cambridge Workshop on Cool Stars, Stellar Systems, and the Sun, eds. C. Johns-Krull, M. K. Browning, & A. A. West, ASP Conf. Ser., 448, 91
Anderson, E., & Francis, C. 2012, Astron. Lett., 38, 331
Artigau, É., Radigan, J., Folkes, S., et al. 2010, ApJ, 718, L38
Banse, K., Crane, P., Grosbol, P., et al. 1982, ESO Messenger, 31, 26
Banse, K., Ponz, D., Ounnas, C., Grosbol, P., & Warmels, R. 1988, Instrumentation for Ground-based Optical Astronomy: Present and Future, ed. L. B. Robinson (New York: Springer), 431
Baraffe, I., Chabrier, G., Allard, F., & Hauschildt, P. H. 1998, A&A, 337, 403
Bayo, A., Rodrigo, C., Barrado Y Navascués, D., et al. 2008, A&A, 492, 277
Bensby, T., Feltzing, S., & Lundström, I. 2003, A&A, 410, 527
Bensby, T., Oey, M. S., Feltzing, S., & Gustafsson, B. 2007, ApJ, 655, L89
Berger, E., Basri, G., Fleming, T. A., et al. 2010, ApJ, 709, 332
Blake, C. H., Charbonneau, D., & White, R. J. 2010, ApJ, 723, 684
Boeche, C., Siebert, A., Williams, M., et al. 2011, AJ, 142, 193
Buckley, D. A. H., Swart, G. P., & Meiring, J. G. 2006, Proc. SPIE, 6267, 62670Z
Burgasser, A. J., Gillon, M., Melis, C., et al. 2014, AJ, in press [arXiv:1410.4288]
Burgh, E. B., Nordsieck, K. H., Kobulnicky, H. A., et al. 2003, Proc. SPIE, 4841, 1463
Burrows, A., Marley, M., Hubbard, W. B., et al. 1997, ApJ, 491, 856
Buzzoni, B., Delabre, B., Dekker, H., et al. 1984, The Messenger, 38, 9
Crawford, S. M., Still, M., Schellart, P., et al. 2010, Proc. SPIE, 7737, 25
Cushing, M. C. Rayner, J. T., & Vacca, W. D. 2005, ApJ, 623, 1115
Dieterich, S. B., Henry, T. J., Golimowski, D. A., Krist, J. E., & Tanner, A. M. 2012, AJ, 144, 64
Dieterich, S. B., Henry, T. J., Jao, W.-Ch., et al. 2014, AJ, 147, 94
Epchtein, N., de Batz, B., Capoani, L., et al. 1997, The Messenger, 87, 27
Evans, D. W., Irwin, M. J., & Helmer, L. 2002,A&A, 395, 347
Faherty, J. K., Burgasser, A. J., West, A. A., et al. 2010, AJ, 139, 176
Feast, M., & Whitelock, P. 1997, MNRAS, 291, 683
Fuchs, B., Breitschwerdt, D., de Avillez, M. A., Dettbarn, C., & Flynn, C. 2006, MNRAS, 373, 993
Gandhi, P., Done, C., Ivanov, V. D., & Huelamo, N. 2013, ATel, 5012, 1
Gehrels, N., Chincarini, G., Giommi, P., et al. 2004, ApJ, 611, 1005
Gelino, C. R., Kirkpatrick, J. D., & Burgasser, A. J. 2004, BAAS, 205, 1113
Haakonsen, C. B., & Rutledge, R. E. 2009, ApJS, 184, 138
Henry, T. J., & Kirkpatrick, J. D. 1990, ApJ, 354, 29
Houk, N. 1978, Michigan catalogue of two-dimensional spectral types for the HD stars, Ann Arbor: Dept. of Astronomy, University of Michigan
Ivanov, V. D., Rieke, G. H., Groppi, C. E., et al. 2000, ApJ, 545, 190
Ivanov, V. D., Rieke, M. J., Engelbracht, C. W., et al. 2004, ApJS, 151, 387
Ivanov, V. D., Minniti, D., Hempel, M., et al. 2013. A&A, 560, A21
Kirkpatrick, J. D. 2003, IAUS, 211, 189
Kirkpatrick, J. D., Henry, T. J., & Simons, D. A. 1995, AJ, 109, 797
Kirkpatrick, J. D., Reid, I. N., Liebert, J., et al. 1999, ApJ, 519, 802
Kirkpatrick, J. D., Reid, I. N., Liebert, J., et al. 2000, AJ, 120, 447
Kirkpatrick, J. D., Cushing, M. C., Gelino, C. R., et al. 2011, ApJS, 197, 19
Kirkpatrick, J. D., Gelino, C. R., Cushing, M. C., et al. 2012, ApJ, 753, 156
Kniazev, A. Y., Zijlstra, A. A., Grebel, E. K., et al. 2008, MNRAS, 388, 1667
Kniazev, A. Y., Vaisanen, P., Mužić, K., et al. 2013, ApJ, 770, 124
Kobulnicky, H. A., Nordsieck, K. H., Burgh, E. B., et al. 2003, Proc. SPIE, 4841, 1634
Leggett, S. K., Burningham, B., Saumon, D., et al. 2010, ApJ, 710, 1627
Lucas, P. W., Tinney, C. G., Burningham, B., et al. 2010, MNRAS, 408, L56
Luhman, K. L. 2013, ApJ, 767, L1
Luhman, K. L. 2014, ApJ, 781, 4
Mamajek, E. E., Bartlett, J. L., Seifahrt, A., et al. 2013, AJ, 146, 154
McLean, I. S., McGovern, M. R., Burgasser, A.-J., et al. 2003, ApJ, 596, 561
Mickaelian, A. M. 2004, A&A, 426, 367
Mohanty, S., & Basri, G. 2003, ApJ, 583, 451
Monet, D. G., Levine, S. E., Canzian, B., et al. 2003, AJ, 125, 984
Moorwood, A., Cuby, J. G., & Lidman, C. 1998, The Messenger, 91, 9
O'Donoghue, D., Buckley, D. A. H., Balona, L. A., et al. 2006, MNRAS, 372, 151
Pickles, A. J. 1998, PASP, 110, 863
Rayner, J. T., Cushing, M. C., & Vacca, W. D. 2009, ApJS, 185, 289
Ribas, I. 2002, A&A, 398, 239
Roeser, S., Demleitner, M., & Schilbach, E. 2010, AJ, 139, 2440
Scholz, R.-D. 2014, A&A, 561, A113
Scholz, R.-D., Bihain, G., Schnurr, O., & Storm, J. 2011, A&A, 532, L5
Scholz, R.-D., Bihain, G., & Storm, J. 2014, A&A, 567, A43
Schönrich, R., Binney, J., & Dehnen, W. 2010, MNRAS, 403, 1829
Simcoe, R. A., Burgasser, A. J., Bernstein, R. A., et al. 2008, Proc. SPIE, 7014,
Simcoe, R. A., Burgasser, A. J., Schechter, P. L., et al. 2013, PASP, 125, 270
Skrutskie, M. F., Cutri, R. M., Stiening, R., et al. 2006, AJ, 131, 1163
Snodgrass, C., Saviane, I., Monaco, L., & Sinclaire, P. 2008, The Messenger, 132, 18
Soubiran, C., Jasniewicz, G., Chemin, L., et al. 2013, A&A, 552, A64
Torres, C. A. O., Quast, G. R., Melo, C. H. F., & Sterzik M. F. 2008, Handbook of Star Forming Regions, Vol. II, ed. B. Riepurth, 757
Tsuboi, Y., Maeda, Y., Feigelson, E. D., et al. 2003, ApJ, 587, L51
van Leeuwen, F. 2007, A&A, 474, 653
Warmels, R. H. 1992, ASPS, 25, 115
Wright, E. L., Eisenhardt, P. R. M., Mainzer, A. K., et al. 2010, AJ, 140, 1868
Wu, Y., Singh, H. P., Prugniel, P., Gupta, R., & Koleva, M. 2011, A&A, 525, A71
Zasov, A. V., Kniazev, A. Y., Pustilnik, S. A., et al. 2000, A&AS, 144, 429